Tumor Model Fitting using Markov Chain Monte Carlo Method

Martin Ferenc Dömény[1,2], Melánia Puskás[1,2], Balázs Gombos[3], András Füredi[3], Gergely Szakács[4], Levente Kovács[1], and Dániel András Drexler[1]

[1]Physiological Controls Research Center, University Research and Innovation Center, Obuda University, Bécsi út 96/b, 1034 Budapest, Hungary, {domeny.martin, puskas.melania, kovacs, drexler.daniel}@uni-obuda.hu
[2]Applied Informatics and Applied Mathematics Doctoral School, Obuda University, Bécsi út 96/b, 1034 Budapest, Hungary
[3]Drug Resistance Research Group, Hungarian Research Network, Magyar tudosok krt 2, 1117, Budapest, Hungary, {gombos.balazs, furedi.andras}@ttk.hu
[4]Center for Cancer Research, Medical University of Vienna, Borschkegasse 8A, 1090 Vienna, Austria, gergely.szakacs@meduniwien.ac.at

Abstract: Accurate mathematical modeling of tumor growth supports understanding treatment effects and experimental planning in preclinical oncology. We apply Markov Chain Monte Carlo (MCMC) methods to estimate parameters of a tumor growth model, defined by ordinary differential equations, using real measurement data from mouse experiments under a predefined dosing schedule. Assuming normally distributed measurement noise, we assess posterior distributions with convergence diagnostics, density plots, and trace plots, while analyzing parameter correlations to evaluate model structure and identifiability. The results highlight that MCMC-based fitting not only provides reliable parameter estimates but also valuable insights into parameter uncertainty, supporting robust modeling strategies in preclinical cancer research.

Keywords: tumor model; personalizing therapy; MCMC; parameter estimation; model fitting

1 Introduction

Mathematical modeling of tumor growth plays a crucial role in understanding cancer dynamics and designing personalized treatment strategies [1, 2]. A variety of models, from empirical growth curves to mechanistic systems of differential equations [3–5], are employed to describe tumor progression. The utility of these models relies heavily on the accuracy of parameter estimation. In preclinical studies, tumor volume is typically estimated using caliper measurements [6], capturing only length and width. Such indirect estimation introduces systematic and stochastic

errors that, if unaccounted for, can lead to biased parameter inference and flawed predictions.

Previous studies demonstrated improved accuracy in identifying key tumor growth parameters through advanced parameter estimation techniques [7]. These approaches, including machine learning-based methods like LSTM recurrent neural networks, provided robust parameter estimates, enhancing the reliability of model-based inference and therapy optimization [8].

In previous works, we have developed both *in vitro* [9] and *in vivo* [10, 11] tumor models, characterized measurement noise from caliper-based methods [12], and applied mixed-effects models [13] to improve parameter estimation. Building on these foundations, we explored personalized treatment design using calibrated tumor models [9, 14]. For example, a genetic algorithm was used to optimize chemotherapy protocols based on estimated parameters, minimizing tumor burden while reducing overall drug exposure [15]. Results indicated that individualized treatment strategies could achieve comparable or superior efficacy relative to conventional maximum-tolerated dose regimens [16].

In order to further enhance personalization, we proposed an AI-based clustering approach to identify individuals with similar tumor dynamics [17] and implemented neural networks capable of rapidly estimating tumor growth parameters from short time-series data [18], significantly reducing computational demands. More recently, we have investigated therapy optimization strategies informed by pharmacokinetics and soft computing techniques [19]. These developments collectively support more reliable, adaptive, and personalized treatment planning [20].

In this study, we employ Markov Chain Monte Carlo (MCMC) methods to perform parameter estimation of tumor models, assuming normally distributed measurement errors. Unlike frequentist approaches, Bayesian methods such as MCMC explicitly quantify parameter uncertainty by generating probability distributions rather than single-point estimates. This allows for the direct incorporation of prior knowledge, better handling of parameter correlations, and clearer interpretation of uncertainty, particularly important given the inherent variability in biological measurements. Our analysis uses tumor volume measurements collected from mice in preclinical experiments, where volumes were calculated using digital calipers capturing length and width over multiple time points [12].

Furthermore, to provide parameter estimation, the MCMC framework enables a detailed analysis of parameter interactions through posterior correlation structures. Such information is valuable for identifying potential redundancies in model structure or limitations in data informativeness. By visualizing joint posterior distributions and examining convergence diagnostics, we can gain a deeper understanding of the robustness and identifiability of the estimated parameters. These insights are essential when model predictions are to be used in applications such as treatment optimization.

2 Preliminaries

2.1 Tumor Growth Model

We used a system of four ordinary differential equations to model tumor progression and the pharmacokinetics/pharmacodynamics of the administered drug. The structure of the model is based on a formal analogy with a chemical reaction, where each variable is interpreted as a fictive species [11]. Let X_1, X_2, X_3, and X_4 denote the living tumor volume, the dead tumor volume, the drug concentration in the central compartment, and the drug concentration in the peripheral compartment, respectively. The biological processes are represented as follows:

$$X_1 \xrightarrow{a} 2X_1, \tag{1}$$

$$X_1 \xrightarrow{n} X_2, \tag{2}$$

$$X_2 \xrightarrow{w} O, \tag{3}$$

$$X_1 + X_3 \xrightarrow{b,\,ED_{50}} X_2, \tag{4}$$

$$X_3 \underset{k_2}{\overset{k_1}{\rightleftarrows}} X_4, \tag{5}$$

$$X_3 \xrightarrow{c} O, \tag{6}$$

where reaction (1) represents tumor cell proliferation with rate a, (2) describes the necrosis of viable tumor cells independent of the drug with rate n, (3) corresponds to the washout of dead tumor tissue with rate w, (4) models the pharmacodynamic effect of the drug with a maximal effect rate b and a median effective dose ED_{50}, (5) accounts for the bidirectional transport of the drug between the central and peripheral compartments with rate constants k_1 and k_2, while (6) describes the elimination of the drug from the central compartment with clearance rate c. The system follows mass-action kinetics [21, 22] for all reactions except the drug effect (4), which is modeled using a Michaelis-Menten kinetics with parameter ED_{50}.

The resulting mathematical model is [10]:

$$\dot{x}_1 = (a-n)x_1 - b\frac{x_1 x_3}{ED_{50}+x_3}, \tag{7}$$

$$\dot{x}_2 = nx_1 + b\frac{x_1 x_3}{ED_{50}+x_3} - wx_2, \tag{8}$$

$$\dot{x}_3 = -(c+k_1)x_3 + k_2 x_4 + u, \tag{9}$$

$$\dot{x}_4 = k_1 x_3 - k_2 x_4. \tag{10}$$

The model also incorporates impulsive inputs representing drug injections. These are formalized as discontinuities in the central drug compartment as

$$x_3(t_i^+) = x_3(t_i^-) + u_i, \tag{11}$$

where u_i [mg/kg] is the amount of injected dose at day t_i. Thus, at t_i, we give the ith

dose, which increases the value of x_3.

The output of the system is the total volume of living and dead tumor cells, denoted as y, which is the sum of the living and dead tumor cells:

$$y = x_1 + x_2 \tag{12}$$

and this is the measured variable in the experiments.

2.2 MCMC in Bayesian Inference

Markov Chain Monte Carlo (MCMC) is a computational method widely used for sampling from complex probability distributions [23, 24]. These methods are used extensively in the literature for modelling model parameter uncertainity [25]. It enables researchers to characterize distributions without requiring explicit analytical knowledge of their mathematical forms. MCMC operates by generating random samples directly from the target distribution, leveraging only the ability to calculate its density for given sample points.

The term MCMC reflects two foundational concepts: Monte Carlo simulation and Markov chains. Monte Carlo methods estimate properties of a probability distribution through analysis of randomly drawn samples. For instance, rather than analytically computing the mean of a normal distribution from its formula, a Monte Carlo approach involves generating numerous random samples from this distribution and calculating their sample mean. This method is particularly advantageous when sampling is straightforward but direct analytical computation is challenging.

The Markov chain component denotes that samples are produced through a sequential process, where each new sample is generated based solely on the immediately preceding sample. This sequential dependence characterizes a Markov process, defined precisely by the property that the current sample depends only on the previous one, independent of earlier samples.

MCMC is especially valuable in Bayesian inference due to its effectiveness in handling posterior distributions that are often analytically intractable. Bayesian inference utilizes observed data to update prior beliefs about parameters, resulting in posterior beliefs. Formally, this updating process is described by Bayes' rule:

$$p(\theta|Y_{obs}) \propto p(Y_{obs}|\theta) \cdot p(\theta), \tag{13}$$

where θ represents the parameters of interest, Y_{obs} denotes the observed data, $p(\theta|Y_{obs})$ is the posterior distribution (the probability of θ after observing the data), $p(Y_{obs}|\theta)$ is the likelihood (the probability of seeing this observation given the parameters (θ)) and $p(\theta)$ represents the prior distribution, which is a hyperparameter of the algorithm, representing the initial knowledge of the parameters. According to Bayes' rule, the posterior is proportional to the product of the likelihood and the prior.

3 Application of MCMC to the Tumor Growth Model

We assigned prior distributions to each model parameter, as summarized in Table 1. To ensure physiological feasibility, we used distributions defined only in the positive domain. Since we lack strong prior knowledge or well-established ranges for most parameters, we specified weakly informative Half-Normal distributions with a standard deviation of $\sigma = 1$. An exception is the observation noise parameter σ_{obs}, for which we used a broader prior with $\sigma = 10$, to account for the measurement error, and any other tumor dynamics that the model fails to capture.

The ODE system was solved numerically with parameters $\theta = [a, b, n, w, ED_{50}]$. The resulting tumor volume trajectory was used as the mean in a normal likelihood:

$$Y_{\text{obs}}(t) \sim \mathcal{N}(\text{ODE}_{\text{sol}}(t), \sigma_{obs}), \tag{14}$$

where $Y_{\text{obs}}(t)$ denotes the observed tumor volume at time t.

The likelihood was modeled assuming additive, independent Gaussian noise with constant variance. Let y_i denote the i-th observation at time t_i, and let μ_i be the model prediction from the ODE solution at the same time. The observation model is

$$y_i = \mu_i + \varepsilon_i, \tag{15}$$

where $\varepsilon_i \sim \mathcal{N}(0, \sigma_{obs}^2)$ are independent measurement errors with unknown standard deviation σ_{obs}.

Under these assumptions, the likelihood for a single observation is given by the Gaussian density

$$p(y_i \mid \mu_i, \sigma_{obs}) = \frac{1}{\sqrt{2\pi\sigma_{obs}^2}} \exp\left(-\frac{(y_i - \mu_i)^2}{2\sigma_{obs}^2}\right). \tag{16}$$

Assuming independence across the N time points, the full likelihood is the product of these densities:

$$\mathscr{L}(\sigma_{obs}; y) = \prod_{i=1}^{N} p(y_i \mid \mu_i, \sigma_{obs}) = (2\pi\sigma_{obs}^2)^{-N/2} \exp\left(-\frac{1}{2\sigma_{obs}^2} \sum_{i=1}^{N} (y_i - \mu_i)^2\right). \tag{17}$$

Taking the natural logarithm yields the log-likelihood:

$$\log \mathscr{L}(\sigma_{obs}; y) = -\frac{N}{2} \log(2\pi\sigma_{obs}^2) - \frac{1}{2\sigma_{obs}^2} \sum_{i=1}^{N} (y_i - \mu_i)^2, \tag{18}$$

where the first term comes from the Gaussian normalization constant and depends only on N and σ_{obs}, while the second term penalizes deviations between model predictions and observations, scaled by the assumed measurement variance. During

Table 1
Prior distributions for model parameters, along with the fixed parameters and the variance of observation noise.

Parameter	**Prior**
a	Half-Normal ($\sigma = 1$)
b	Half-Normal ($\sigma = 1$)
n	Half-Normal ($\sigma = 1$)
w	Half-Normal ($\sigma = 1$)
ED_{50}	Half-Normal ($\sigma = 1$)
c	1.8211
k_1	14.0080
k_2	136.2781
σ_{obs}	Half-Normal ($\sigma = 10$)

inference, this log-likelihood is combined with the prior distributions to form the posterior, guiding parameter estimation toward values that yield predictions consistent with the observed data within the assumed noise level.

4 Results

In order to create the results, the PyMC library [26] was utilized, providing the framework for the Bayesian analysis. For all chains, we used 5000 burn-in samples and 5000 real samples, and we used 8 chains in parallel. The burn-in samples are discarded, so they do not contribute to the posterior samples at the end. They are used to give enough time for the Markov Chain to settle into its stationary state. The number of chains was selected to balance between convergence diagnostics reliability and the limitations of the computing environment, while the per-chain sample size was chosen to provide sufficient effective sample size for posterior inference within a reasonable runtime. For the fitting, we used tumor volume measurements from mice experiments [1]. The measurements were carried out using digital caliper.

Figure 1 shows a posterior predictive check, comparing the Bayesian model's predicted tumor volume dynamics against observed data. The x-axis represents time (in days), and the y-axis shows tumor volume. The median trajectory closely follows the measured tumor volume trend, capturing both the rapid rise and subsequent decline in volume. This suggests that the model effectively captures the overall dynamics of tumor response. In Table 2, we can observe the metrics used to determine the goodness of fit. The Relative Mean Squared Error is 66.85. The median fit tends to undershoot the data by roughly half of the observed volume, consistent with the tight 90% band sitting just below many points in the early phase. The median-parameter trajectory captures the overall dynamics very well ($R^2 \approx 0.91$), but the large negative MPE tells us it sits systematically below the data, particularly visible around the growth peak. Residual scatter (MAE and RMSE) is

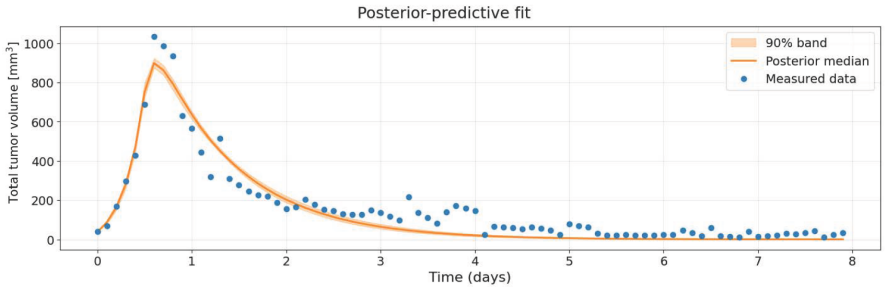

Figure 1
Posterior predictive fit of the tumor volume model. The blue dots represent the observed measurements over time. The orange line represents the posterior median prediction, while the shaded region around the median corresponds to the 90% credible interval (There is a 90% probability that the true value is within the interval (given the data)). The close alignment between data and prediction indicates a good fit and well-calibrated uncertainty.

Table 2
Goodness-of-fit metrics for the posterior–median parameter set

Metric	Symbol	Value
Root-mean-square error	RMSE	**66.85**
Mean absolute error	MAE	52.58
Mean percentage error	MPE	-52.16%
Coefficient of determination	R^2	0.905

moderate; a few outliers inflate RMSE relative to MAE.

The posterior predictive fit was illustrated for a single representative mouse to demonstrate the feasibility of the method. In our dataset, the majority of individual tumor growth curves follow a similar qualitative pattern, with initial growth followed by regression, so the selected example is representative of the general trend observed across animals. Given the high computational cost of full posterior predictive checks for all mice, we limited the detailed demonstration to one case in this study. In future work, we plan to extend the analysis to the full dataset to assess predictive performance at the population level.

Refining the noise model (e.g., using a noise model with heteroskedastic standard deviation) or using the posterior predictive mean instead of the single median curve would likely reduce bias and improve the error metrics. This expectation is supported by our previous work on caliper measurement error modeling [12, 27], where we showed that the measurement noise variance is not constant but depends on tumor size, being higher for small tumors and lower for large tumors. A heteroskedastic noise model could capture this size-dependent measurement error, potentially reducing bias in parameter estimation and improving predictive accuracy.

Figure 2 shows the posterior trace plots for the five model parameters and the σ

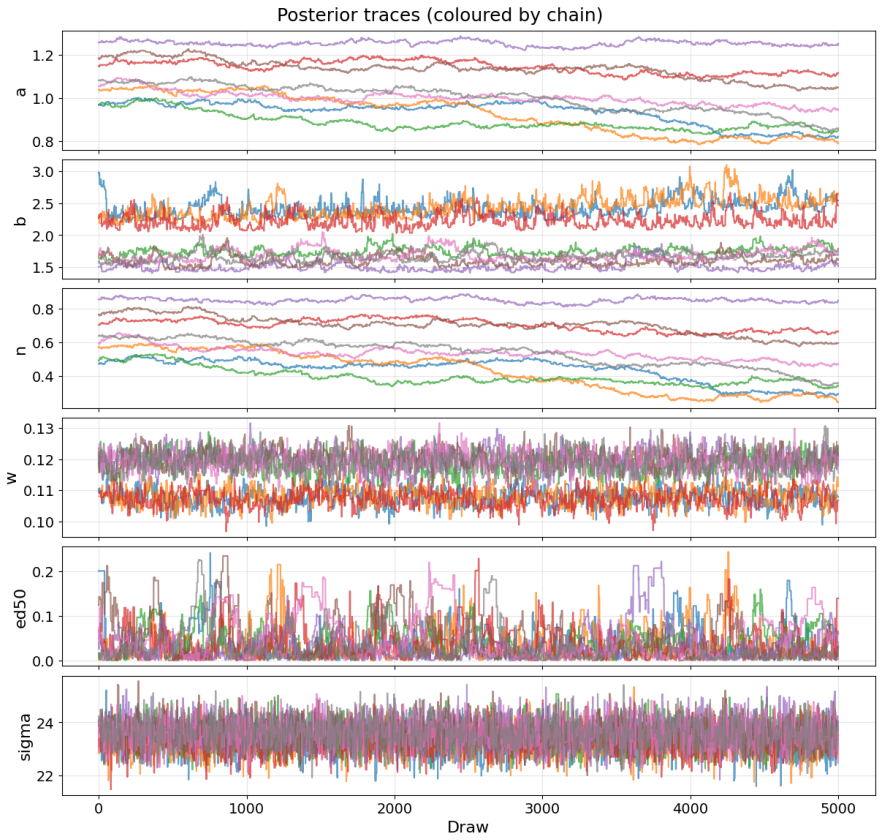

Figure 2
Trace plots for six model parameters over 5000 MCMC draws, with each color representing a separate chain. Parameters a, b, and n exhibit slow mixing and inter-chain separation, indicating convergence difficulties. In contrast, parameters w, ED_{50}, and σ show well-mixed chains, suggesting reliable posterior sampling for these quantities.

parameter of the measurement noise, sampled by multiple MCMC chains. Each colored line corresponds to one of the parallel chains across 5000 iterations (draws). Trace plots are essential for assessing the convergence and mixing of the MCMC sampler. Well-mixed chains should resemble "stationary noise," fluctuating around a consistent central value without strong drift or structure.

The chains for a and n display slow convergence and poor mixing. The traces exhibit clear separation between chains, suggesting that they may not have converged to a common stationary distribution. There appears to be a strong dependence between these parameters (also visible in Figure 3), which likely complicates their joint sampling. The trace for b shows two separate clusters of chains, indicating a bimodal shape in the posterior. The trace plots for w and ED_{50} appear noisier but relatively well mixed, with overlapping chains and no evident drift. Although ED_{50}

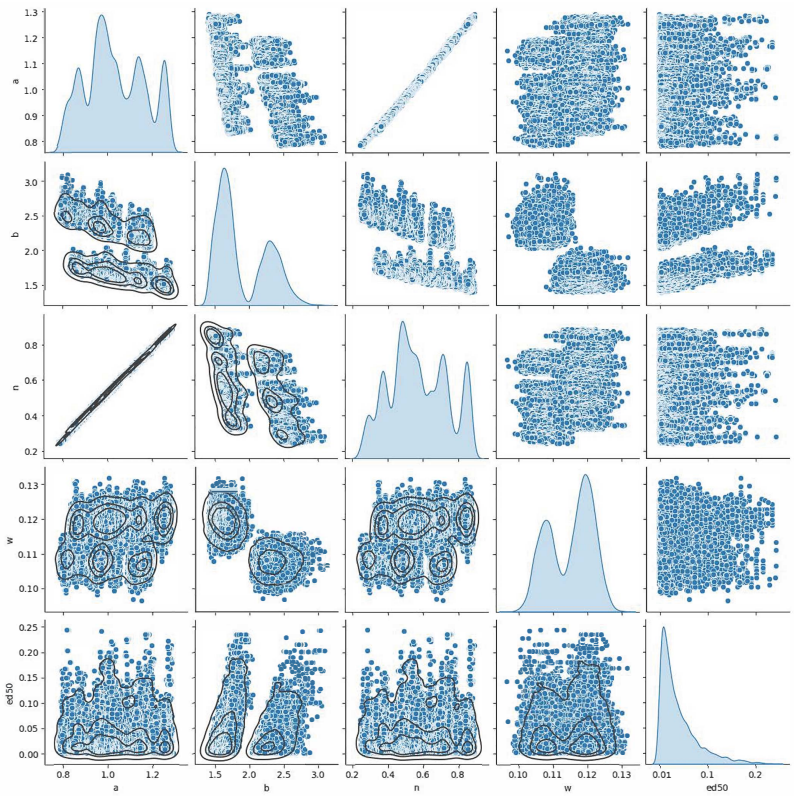

Figure 3
Pairwise posterior distributions of the tumor model parameters obtained via MCMC. Diagonal plots show marginal distributions; off-diagonal plots display joint distributions with density contours. A strong correlation is observed between parameters a and n, while ED_{50} exhibits a right-skewed, near-zero distribution. The multimodal nature of several parameters indicates a complex posterior landscape.

shows more variability, this may reflect genuine posterior variability due to sparse information content in the data. The noise parameter σ shows excellent mixing, with overlapping chains exhibiting stationary behavior and no sign of autocorrelation or drift. This confirms that the noise scale of the model is well-identified and efficiently sampled.

In Figure 3, a corner plot summarizes the joint and marginal posterior distributions of five parameters involved in the tumor model. It provides insights into parameter uncertainty, correlations, and identifiability. Each diagonal subplot shows the marginal posterior distribution of a parameter. These distributions represent the individual uncertainty of each parameter after conditioning on the observed data. Parameters a and n show multi-modal or rugged distributions, suggesting possible identifiability issues or complex posterior structure. Parameter b has a few sharp

peaks, indicating multiple modes. Parameters w and ED_{50} exhibit skewed and/or heavy-tailed distributions, particularly ED_{50}, which is sharply right-skewed and near-zero.

Each subplot off the diagonal visualizes the pairwise joint posterior distributions between two parameters. Parameters a and n have nearly perfect positive correlation (tight linear relationship), implying strong collinearity. This can make the independent estimation of these parameters difficult. Parameter b shows nontrivial interactions with both a and n, potentially indicating a non-linear dependency structure. Parameters w and ED_{50} show little to no correlation with other parameters, evidenced by the circular scatter and uniform contour spread. These parameters may be more independently estimable from the data. The joint posterior distributions involving ED_{50} are dispersed, showing high density near zero, again suggesting identifiability issues or prior influence. The presence of multiple modes, especially in b, n, and possibly w, suggests that the posterior distribution is non-Gaussian and possibly multi-modal.

Previous works on parameter estimation for this tumor model have employed approaches such as mixed-effects modeling and soft computing techniques [8], including artificial neural networks combined with local search methods [28, 29]. While these methods can provide point estimates efficiently, they do not directly quantify the uncertainty of the estimates. In contrast, MCMC returns full posterior distributions for each parameter, allowing uncertainty quantification and credible interval estimation alongside point estimates. This feature is particularly valuable in therapy optimization, where understanding the reliability of parameter values can influence dosing decisions.

Conclusion

This study demonstrates the feasibility and utility of Bayesian parameter estimation using Markov Chain Monte Carlo (MCMC) methods for calibrating our *in vivo* tumor growth model to preclinical measurement data. The results highlight that the MCMC framework enables the estimation of multiple parameters while simultaneously quantifying their uncertainties and mutual dependencies.

The posterior distributions revealed varying levels of identifiability among parameters. While some, such as the residual error standard deviation (σ) and the drug efficacy parameter (ED_{50}), exhibited broad and skewed distributions with dense regions near zero, others showed strong correlations, particularly between the growth-related parameters (a, b, n). The trace plots and posterior predictive checks confirmed reasonable convergence and model fit, capturing the declining tumor volume observed in the data.

The correlation structure observed in the joint posterior distributions suggests potential issues with parameter redundancy or a lack of informativeness in the data. The presence of multimodality in some marginals indicates that further constraints or structural refinement may be necessary to improve identifiability.

Future work will focus on extending the model to include a validated noise

model from our previous research [12], as real experimental data often exhibit both systematic and random errors, which are currently only partially accounted for. Furthermore, we aim to investigate how different dosing schedules influence parameter correlations and identifiability. Such extensions are expected to enhance model realism and support more robust applications in treatment design and optimization.

Acknowledgment

This project has been supported by the Hungarian National Research, Development and Innovation Fund of Hungary, financed under the TKP2021-NKTA-36 funding scheme. This research was partially supported by the European Union (EU HORIZON-MSCA-2023-SE-01-01) and the Hungarian NRDI program (2020-2.1.1-ED-2024-00346) within the DSYREKI: Dynamical Systems and Reaction Kinetics Networks project. The work of Dániel András Drexler was supported by the Starting Excellence Researcher Program of Obuda University, Budapest Hungary. Melánia Puskás is also with the Obuda University, Applied Informatics and Applied Mathematics Doctoral School, Budapest, Hungary. Martin Ferenc Dömény and Melánia Puskás were supported by the 2024-2.1.1 University Research Scholarship Program of the Ministry for Culture and Innovation from the source of the National Research, Development and Innovation Fund. The authors acknowledge the support of the National Talent Program under the NTP-HHTDK-23-0077 project.

References

[1] L. Kovács, T. Ferenci, B. Gombos, A. Füredi, I. Rudas, G. Szakács, and D. A. Drexler. Positive impulsive control of tumor therapy—a cyber-medical approach. *IEEE Transactions on Systems, Man, and Cybernetics: Systems*, 54(1):597–608, 2024.

[2] C.-B. Chng, K. Koenig, P.-M. Wong, M. Wang, J. Wu, and C.-K. Chui. Towards a pharmaceutical cyber-physical systems based automated drug discovery workcell. *Acta Polytechnica Hungarica*, 21(9):233–246, 2024.

[3] P. M. Altrock, L. L. Liu, and F. Michor. The mathematics of cancer: integrating quantitative models. *Nature Reviews. Cancer*, 15(12):730–745, 2015.

[4] A. M. Jarrett, E. A. B. F. Lima, D. A. Hormuth, M. T. McKenna, X. Feng, D. A. Ekrut, A. C. M. Resende, A. Brock, and T. E. Yankeelov. Mathematical models of tumor cell proliferation: A review of the literature. *Expert Review of Anticancer Therapy*, 18(12):1271–1286, 2018.

[5] J. S. Lowengrub, H. B. Frieboes, F. Jin, Y.-L. Chuang, X. Li, P. Macklin, S. M. Wise, and V. Cristini. Nonlinear modelling of cancer: bridging the gap between cells and tumours. *Nonlinearity*, 23(1):R1–R9, 2010.

[6] M. Puskás, B. Gergics, L. Kovács, and D. A. Drexler. Tumor volume measurements in animal experiments: Current approaches and their

limitations. In *System Dependability - Theory and Applications*, pages 206–217. Springer Nature Switzerland, 2024.

[7] D. A. Drexler, M. F. Dömény, T. Ferenci, B. Gergics, L. Kisbenedek, M. Puskás, T. D. Szűcs, and L. Kovács. Cyber-medical systems in chemotherapy treatment optimization. In L. Kovács, T. Haidegger, and A. Szakál, editors, *Recent Advances in Intelligent Engineering: Volume Dedicated to Imre J. Rudas' Seventy-Fifth Birthday*, pages 245–269. Springer Nature Switzerland, 2024.

[8] B. Gergics, M. Puskas, L. Kisbenedek, M. F. Domeny, L. Kovacs, and D. A. Drexler. Chemotherapy optimization and patient model parameter estimation based on noisy measurements. *Acta Polytechnica Hungarica*, 21(10):475–494, 2024.

[9] B. Gergics, B. Gombos, F. Vajda, A. Füredi, G. Szakács, and D. A. Drexler. Pharmacodynamics modeling based on in vitro 2D cell culture experiments. In *Proceedings of the 2022 IEEE International Conference on Systems, Man, and Cybernetics (SMC)*, pages 2409–2414, 2022.

[10] D. A. Drexler, T. Ferenci, A. Füredi, G. Szakács, and L. Kovács. Experimental data-driven tumor modeling for chemotherapy. In *Proceedings of the 21st IFAC World Congress*, pages 16466–16471, 2020.

[11] D. A. Drexler, T. Ferenci, A. Lovrics, and L. Kovács. Tumor Dynamics Modeling based on Formal Reaction Kinetics. *Acta Polytechnica Hungarica*, 16:31–44, 2019.

[12] M. Puskás and D. A. Drexler. Modeling the error of caliper measurements in animal experiments. *IEEE Access*, 13:54836–54852, 2025.

[13] M. Fidler, Y. Xiong, R. Schoemaker, J. Wilkins, M. Trame, T. Post, and W. Wang. *nlmixr: Nonlinear Mixed Effects Models in Population Pharmacokinetics and Pharmacodynamics*, 2018. R package version 1.0.0-7.

[14] M. F. Dömény, M. Puskás, L. Kovács, T. T. Mac, and D. A. Drexler. Detecting critical supervision intervals during in silico chemotherapy treatments. *Acta Polytechnica Hungarica*, 21(9):247–261, 2024.

[15] M. F. Dömény, M. Puskás, L. Kovács, and D. A. Drexler. Population-based chemotherapy optimization using genetic algorithm. In *2023 IEEE 21st Jubilee International Symposium on Intelligent Systems and Informatics (SISY)*, pages 000023–000028, 2023.

[16] J. Sapi. Finding maximum tolerated dose in phase i oncology clinical trials with bayesian methods. *Acta Polytechnica Hungarica*, 21(6):129–145, 2024.

[17] L. Kisbenedek, M. Puskás, L. Kovács, and D. A. Drexler. Clustering-based parameter estimation of a tumor model. In *2023 IEEE 21st Jubilee International Symposium on Intelligent Systems and Informatics (SISY)*, pages 000043–000048, 2023.

[18] L. Kisbenedek, M. Puskás, D. A. Drexler, and L. Kovács. Autoencoder-based architecture for parameter estimation of a tumor model. In *2024 IEEE 24th International Symposium on Computational Intelligence and Informatics (CINTI)*, pages 215–220, 2024.

[19] M. Puskás, B. Gergics, A. Ládi, and D. A. Drexler. Parameter estimation from realistic experiment scenario using artificial neural networks. In *2022 IEEE 16th International Symposium on Applied Computational Intelligence and Informatics (SACI)*, pages 161–168, 2022.

[20] D. A. Drexler, B. Gergics, M. Puskás, T. P. Haidegger, and L. A. Kovács. Personalized therapy using drug delivery devices. *IFAC-PapersOnLine*, 58(24):550–555, 2024. 12th IFAC Symposium on Biological and Medical Systems BMS 2024.

[21] P. Érdi and J. Tóth. *Mathematical Models of Chemical Reactions. Theory and Applications of Deterministic and Stochastic Models*. Princeton University Press, Princeton, New Jersey, 1989.

[22] J. Tóth, A. L. Nagy, and D. Papp. *Reaction kinetics: exercises, programs and theorems*. Springer, 2018.

[23] D. Gamerman and H. F. Lopes. *Markov Chain Monte Carlo: Stochastic Simulation for Bayesian Inference, Second Edition*. Chapman and Hall/CRC, May 2006.

[24] W. R. Gilks, S. Richardson, and D. Spiegelhalter. *Markov Chain Monte Carlo in Practice*. Chapman and Hall/CRC, December 1995.

[25] E. Antonini, G. Mu, S. Sansaloni-Pastor, V. Varma, and R. Kabak. Mcmc methods for parameter estimation in ode systems for car-t cell cancer therapy. *Cancers*, 16(18):3132, September 2024.

[26] O. Abril-Pla, V. Andreani, C. Carroll, L. Dong, C. J. Fonnesbeck, M. Kochurov, R. Kumar, J. Lao, C. C. Luhmann, O. A. Martin, M. Osthege, R. Vieira, T. Wiecki, and R. Zinkov. Pymc: a modern, and comprehensive probabilistic programming framework in python. *PeerJ Computer Science*, 9:e1516, September 2023.

[27] M. Puskás, T. Ferenci, L. Kovács, and D. A. Drexler. Systematic errors in tumor volume estimation: Noise modeling in digital caliper measurements. In *2025 IEEE 19th International Symposium on Applied Computational Intelligence and Informatics (SACI)*, pages 000175–000182, 2025.

[28] L. Kisbenedek, M. Puskás, L. Kovács, and D. A. Drexler. Indirect supervised fine-tuning of a tumor model parameter estimator neural network. In *2023 IEEE 17th International Symposium on Applied Computational Intelligence and Informatics (SACI)*, pages 000109–000116, 2023.

[29] M. Puskás and D. A. Drexler. Tumor model parameter estimation for therapy optimization using artificial neural networks. In *2021 IEEE International*

Conference on Systems, Man, and Cybernetics (SMC), pages 1254–1259, 2021.